research papers

Magnetic behaviour of synthetic Co_2SiO_4

Andrew Sazonov,[a,b]* Martin Meven,[b] Vladimir Hutanu,[a,b] Gernot Heger,[a] Thomas Hansen[c] and Arsen Gukasov[d]

[a]Institut für Kristallographie, Rheinisch-Westfälische Technische Hochschule (RWTH) Aachen, D-52056 Aachen, Germany, [b]Forschungsneutronenquelle Heinz Maier-Leibnitz (FRM II), Technische Universität München (TUM), D-85747 Garching, Germany, [c]Institut Laue–Langevin (ILL), F-38042 Grenoble, France, and [d]Laboratoire Léon Brillouin (LLB), CEA/Saclay, F-91191, Gif-sur-Yvette, France

Correspondence e-mail:
andrew.sazonov@frm2.tum.de

Synthetic Co_2SiO_4 crystallizes in the olivine structure (space group *Pnma*) with two crystallographically non-equivalent Co positions and shows antiferromagnetic ordering below 50 K. We have investigated the temperature variation of the Co_2SiO_4 magnetic structure by means of non-polarized and polarized neutron diffraction for single crystals. Measurements with non-polarized neutrons were made at 2.5 K (below T_N), whereas polarized neutron diffraction experiments were carried out at 70 and 150 K (above T_N) in an external magnetic field of 7 T parallel to the *b* axis. Additional accurate non-polarized powder diffraction studies were performed in a broad temperature range from 5 to 500 K with small temperature increments. Detailed symmetry analysis of the Co_2SiO_4 magnetic structure shows that it corresponds to the magnetic (Shubnikov) group *Pnma*, which allows the antiferromagnetic configuration (G_x, C_y, A_z) for the 4*a* site with inversion symmetry $\bar{1}$ (Co1 position) and ($0,C_y,0$) for the 4*c* site with mirror symmetry *m* (Co2 position). The temperature dependence of the Co1 and Co2 magnetic moments obtained from neutron diffraction experiments was fitted in a modified molecular-field model. The polarized neutron study of the magnetization induced by an applied field shows a non-negligible amount of magnetic moment on the oxygen positions, indicating a delocalization of the magnetic moment from Co towards neighbouring O owing to superexchange coupling. The relative strength of the exchange interactions is discussed based on the non-polarized and polarized neutron data.

1. Introduction

Orthosilicate olivine $(Mg_{1-x}Fe_x)_2SiO_4$ is a major phase of the earth's upper mantle, which represents nearly 20% of the planet's volume. Knowledge of its thermodynamic properties is crucial for undertaking many mineralogical, petrological and geophysical investigations. Besides the fundamental importance for geologists and mineralogists, olivines display a surprising variety of chemical and physical properties. A large number of studies exist on olivine's structural and crystal-chemical properties, as well as lattice-dynamical behaviour (see *e.g.* Haiber *et al.*, 1997; Henderson *et al.*, 2001; Lin, 2001; Wilke *et al.*, 2001; Rinaldi *et al.*, 2005, and references therein). Owing to the presence of 3*d* transition metal cations *M* (Fe^{2+}, Co^{2+}, Mn^{2+} and Ni^{2+}), the magnetic and electronic properties of the M_2SiO_4 olivines have also been studied rather intensively (see *e.g.* Kato *et al.*, 1995; Hagemann *et al.*, 2000; Cococcioni *et al.*, 2003; Jiang & Guo, 2004, and references therein).

M_2SiO_4 compounds crystallizing in the olivine structure are characterized by a distorted hexagonal close-packed array of

oxygen anions in which one-eighth of the tetrahedral interstices are filled by silicon and one-half of the octahedral interstices are occupied by the divalent metal cation M. The olivine-type silicates have an orthorhombic crystal structure with the space group *Pnma* (No. 62 according to Hahn, 1995), in which four formula units are contained in the unit cell ($Z = 4$). The Si atoms are coordinated by four O atoms to form isolated SiO_4 tetrahedra connected *via* divalent cations M. These cations are surrounded by six O atoms and occupy two distinct octahedral sites; $M1$ is located on a center of symmetry and $M2$ on a mirror plane. A more detailed description can be found elsewhere (Sazonov *et al.*, 2008).

Most of the studies provided on the olivine-type oxides have been performed at or above room temperature and at high pressure. In spite of these investigations, which have shed much light on the structural, crystal-chemical, lattice dynamic, magnetic and thermodynamic properties of the olivine group of minerals, uncertainties and gaps in knowledge still persist. One of the less-studied olivine-type silicates is the synthetic cobalt olivine, Co_2SiO_4.

Summarizing the various studies, it was proposed that olivines are magnetically ordered at low temperatures with the magnetic cell equal to the crystallographic cell. The magnetic structure is quite complex and the magnetic moments and their temperature dependences are different for the $M1$ and $M2$ sites. Considering the case of Co-olivine, Nomura *et al.* (1964) determined, using powder magnetic susceptibility measurements as well as neutron powder diffraction data, that a paramagnetic to antiferromagnetic phase transition occurs in Co_2SiO_4 at ~ 49 K. Robie *et al.* (1982) observed in heat-capacity measurements of Co_2SiO_4 a sharp λ peak at ~ 50 K corresponding to this transition. In our previous paper (Sazonov *et al.*, 2008) we determined precisely changes in the crystal structure of Co_2SiO_4 in the temperature range from 2.5 to 300 K by means of X-ray powder and single-crystal neutron diffraction measurements. The high accuracy in the determination of the lattice parameters, the atomic positions and the atomic displacement parameters (ADPs) in that study was essential to correctly interpret the magnetization density distribution obtained in our experiments with polarized neutrons on a Co_2SiO_4 single crystal. Moreover, the magnetic properties of Co_2SiO_4 have been investigated in more detail by both neutron diffraction and magnetization measurements. We also present the result of a complete symmetry analysis of the possible magnetic structures for Co_2SiO_4 which have not been discussed before in detail, while the different magnetic structure models for Co_2SiO_4 have already been proposed earlier (Nomura *et al.*, 1964; Kondo & Miyahara, 1966; Lottermoser & Fuess, 1988).

2. Experimental

2.1. Sample preparation

A 5 g sample of Co_2SiO_4 was prepared by conventional ceramic synthesis for the neutron powder diffraction measurements. Stoichiometric amounts of the appropriate oxides CoO and SiO_2 were carefully ground in an agate mortar to a fine homogeneous black powder. The mixture was then pressed to a pellet and heated in air in an Al_2O_3 crucible to 1400 K at a rate of ~ 100 K h^{-1}. After the initial 48 h at 1400 K, the sample was reground and the heating procedure was repeated. Finally, the sample was cooled in the furnace by switching off the power. Thus, a violet powder was obtained. The laboratory X-ray powder diffraction tests indicated a single phase product.

The same procedure was initially followed to obtain material for the single-crystal growth. After the synthesis, the powder was re-ground and pressed into a rod which was finally sintered at the same conditions as described above. Parts of this rod were then used as the feed and seed rods during the crystal growth procedure. Crystal growth was performed by the floating-zone method using a mirror furnace (see Sazonov *et al.*, 2008, for more detailed information).

2.2. Neutron diffraction studies

2.2.1. Non-polarized neutron diffraction. Accurate lattice parameters of Co_2SiO_4 were obtained from neutron powder diffraction. These measurements were performed using the D20 diffractometer (ILL, France) in its high-resolution mode. The neutron wavelength was $\lambda = 1.87$ Å. Approximately 2 g of Co_2SiO_4 were loaded into a standard ILL-type 7-mm vanadium can. Data were collected every 6 min with a fixed ramp rate of 1 K for 6 min in the temperature range 5–100 K and 4 K for 6 min in the range 100–500 K. This procedure of fixed ramp rate and continuous data collection was applied to reduce the temperature gradient effects across the sample. Each diffraction pattern was measured in the angular range $10 < 2\theta < 150°$ with 2θ steps of 0.1°. Structural parameters of Co_2SiO_4 were obtained from Rietveld refinements using the computer program *FULLPROF* (Rodríguez-Carvajal, 1993).

To obtain a higher accuracy in the determination of both the nuclear and magnetic structure parameters, a small Co_2SiO_4 single crystal of $3 \times 2 \times 2$ mm was cut from the large as-grown crystal. The sample was studied on the four-circle diffractometer HEiDi (Meven *et al.*, 2007) at the hot-neutron source of the FRM II reactor (TUM, Germany). Detailed experimental and refinement data for these single-crystal neutron diffraction measurements at 2.5, 55 and 300 K can be found elsewhere (Sazonov *et al.*, 2008). These results were used as a reference for the neutron powder diffraction investigations.

2.2.2. Polarized neutron diffraction. The magnetization density distribution for Co_2SiO_4 was obtained from polarized neutron single-crystal diffraction. These measurements were performed at the ORPHÉE reactor (LLB, France). Polarized neutron flipping ratios were measured on the lifting-counter diffractometer 5C1 using neutrons with wavelength $\lambda = 0.845$ Å obtained with a Heusler-alloy monochromator. Data were collected in an external field of 7 T above the ordering temperature ($T_N \simeq 50$ K) at 70 and 150 K. For both temperatures, one set of flipping ratios was measured with the field applied parallel to the crystallographic b axis. The higher-order contamination was suppressed by means of an erbium

filter to a level of less than 0.01%. The Maximum Entropy method (MEM) computer program *MEND* (Sakata *et al.*, 1993) was used to calculate magnetization densities from the single-crystal diffraction data.

2.2.3. Magnetic susceptibility studies. The d.c. magnetization measurements were performed using a MPMS-5 SQUID magnetometer (Quantum Design, USA) at the Berlin Neutron Scattering Center (BENSC), Hahn Meitner Institute (HMI), Berlin, Germany. For these measurements, a single-crystal sample with dimensions of $2 \times 2 \times 2$ mm^3 and a mass of 37.1 mg was cut from the as-grown Co_2SiO_4 crystal, with the three axes of the unit cell along the edges of the cube. The sample was placed in a plastic container and brought into a measuring position using a straw. The temperature dependences of the magnetization $M(T)$ were measured on warming from 5 to 330 K in a field of 5 T after a field cooling (FC) or zero-field cooling (ZFC) procedure. The difference between the FC and ZFC measurements was found to be negligible.

3. Results and discussion

3.1. Crystal structure

Some important aspects of the olivine structure (see *e.g.* Sazonov *et al.*, 2008, and references therein) necessary for understanding the magnetic structure of Co_2SiO_4 are summarized below. The Co_2SiO_4 crystal structure can be considered as an arrangement of the CoO_6 octahedra in layers perpendicular to the *c* axis at $z = 0$ and $z = 0.5$. The Co1 ions are located exactly in these layers, whereas the Co2 ions are slightly shifted along the *c* axis. The $Co1O_6$ octahedra are interconnected by common edges and form single chains along the *b* axis (Figs. 1 and 2). The $Co2O_6$ octahedra are attached on alternate sides to the $Co1O_6$ chains in a way that the whole arrangement of $Co1O_6$ and $Co2O_6$ octahedra forms zigzag chains along the *b* axis. A section of the resulting three-dimensional arrangement of the Co^{2+} ions forming zigzag chains in layers perpendicular to the *c* axis is shown in Fig. 1. These chains are separated by SiO_4 tetrahedra (not shown for simplicity). Besides the two $Co1O_6$ neighbouring octahedra (Fig. 2*a*) there are four corner-shared $Co2O_6$ octahedra and two common-edge $Co2O_6$ octahedra (Fig. 2*b*) for every $Co1O_6$. On the other hand, each $Co2O_6$ octahedron has four

$Co2O_6$ neighbours with common corners (Fig. 2*c*). Moreover, there are four $Co1O_6$ neighbour octahedra connected to $Co2O_6$ by common corners and two by common edges (Fig. 2*d*). According to our single-crystal neutron diffraction measurements, the interatomic distances between Co^{2+} within the zigzag chain lie between 2.9936 (1) and 3.2095 (5) Å at room temperature. The Co—Co distances between the near-neighbour chains are in the range from 3.6138 (5) to 3.8672 (5) Å. All other distances between the Co ions are larger than the double spacing between the layers [4.7785 (1) Å]. In general, the variation of the above-mentioned interatomic distances with temperature is smaller than half a percent in the range from 300 K down to 2.5 K.

3.2. Magnetic susceptibility studies

The d.c. magnetic susceptibility χ of a cobalt olivine single crystal is plotted as a function of temperature in Fig. 3. Hereafter, we denote $\chi(T)$ with an applied field along the *a*, *b* and *c* crystallographic axes by χ_a, χ_b and χ_c. The average magnetic susceptibility χ_{av}, defined as $\chi_{av} = (\chi_a + \chi_b + \chi_c)/3$, is shown in the inset to Fig. 3.

3.2.1. Paramagnetic region. The inverse magnetic susceptibilities $\chi_\alpha^{-1}(T)$ ($\alpha = a, b, c$) are linear in the temperature range from ~ 80 K up to 330 K indicating paramagnetic behaviour. The extrapolations of the linear portion of $\chi_\alpha^{-1}(T)$
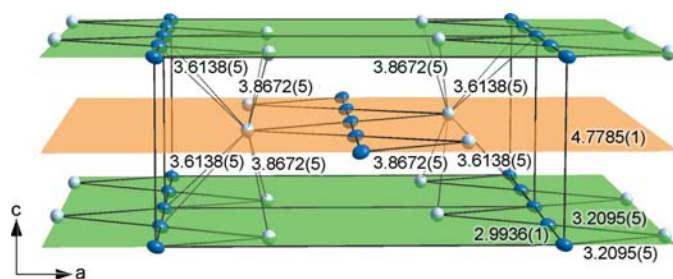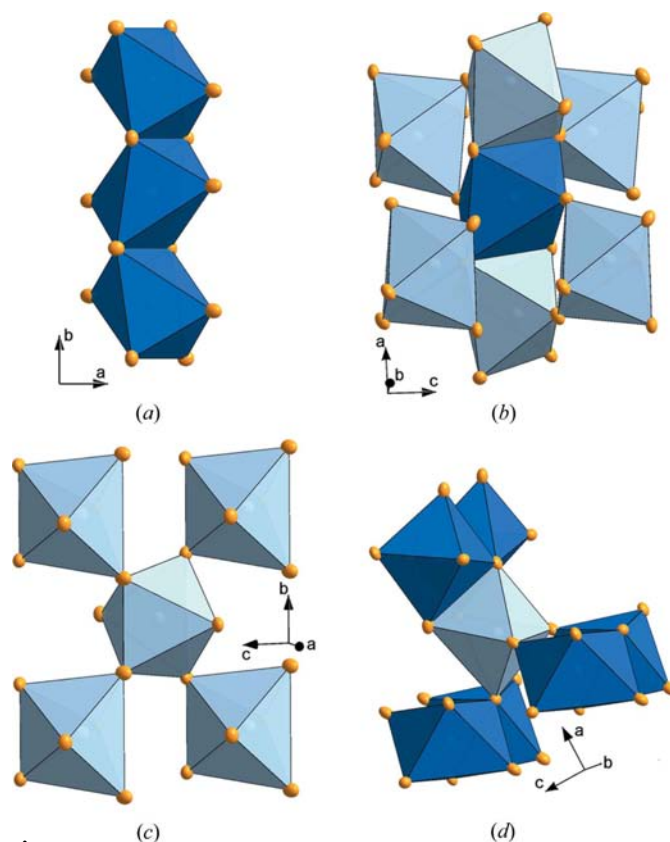

Figure 1
Perspective drawing of the arrangement of the Co^{2+} ions in layers perpendicular to the *c* axis (space group *Pnma*) of Co_2SiO_4. Some Co—Co distances are marked for clarity.

Figure 2
All possible arrangements of the CoO_6 octahedra in Co_2SiO_4 (see text for details). (*a*) $Co1O_6$ neighbours of $Co1O_6$, (*b*) $Co2O_6$ neighbours of $Co1O_6$, (*c*) $Co2O_6$ neighbours of $Co2O_6$ and (*d*) $Co1O_6$ neighbours of $Co2O_6$.

Table 1
The Curie–Weiss temperatures θ_{CW}, Curie constants C and effective magnetic moments μ_{eff} determined from the Curie–Weiss fits of high-temperature portions of the magnetic susceptibilities $\chi_\alpha(T)$ ($\alpha = a, b, c$) for Co_2SiO_4.

α	θ_{CW}	C (emu K mol^{-1})	μ_{eff} (μ_B)
a	-116.4 ± 0.9	2.87 ± 0.01	4.79 ± 0.01
b	-17.9 ± 1.5	3.15 ± 0.03	5.02 ± 0.03
c	-49.5 ± 0.6	2.91 ± 0.01	4.82 ± 0.01
Average†	-45.7 ± 0.5	2.88 ± 0.01	4.80 ± 0.01

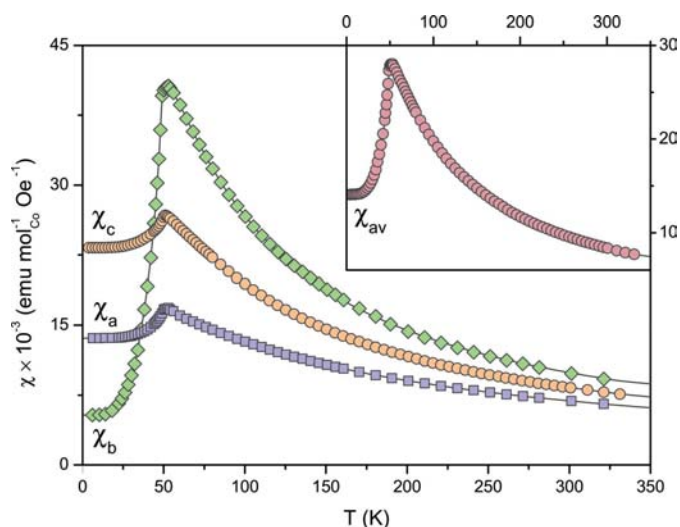† From the fit of the average magnetic susceptibility χ_{av} (see text).

intersect the negative temperature axis implying that the dominant magnetic interactions are antiferromagnetic in nature. The susceptibility strongly depends on the direction of the applied external magnetic field. That is, the three $\chi_\alpha(T)$ curves do not coincide at least up to 330 K. This indicates a strong magnetic anisotropy in the paramagnetic phase, which can be studied by fitting the observed $\chi(T)$ curves from 80 to 330 K to the Curie–Weiss law

$$\chi(T) = \frac{C}{T - \theta_{CW}}, \tag{1}$$

where C is the Curie constant and θ_{CW} is the Curie–Weiss temperature.

Any constant, temperature-independent susceptibility terms, such as diamagnetic, Pauli paramagnetic or instrumental background effects, were taken to be negligible. The best fits were obtained with parameters listed in Table 1.

We would like to compare the $\chi(T)$ data reported by Hagemann *et al.* (2000) for their polycrystalline Co_2SiO_4 sample with our single-crystal data. For this purpose, we fitted the $\chi_{av}(T)$ curve (see inset to Fig. 3) to the Curie–Weiss law

Figure 3
Temperature dependencies of the d.c. magnetic susceptibilities $\chi_\alpha(T)$ ($\alpha = a, b, c$) of Co_2SiO_4 in an external field of 5 T applied along the crystallographic axes a, b and c. The inset shows the average magnetic susceptibility χ_{av}, defined as $\chi_{av} = (\chi_a + \chi_b + \chi_c)/3$.

[equation (1)]. The obtained value of $\theta_{CW} = -45.7 \pm 0.5$ K is very close to that of -45.5 K (Hagemann *et al.*, 2000). The fitted individual $\theta_{CW}^\alpha(T)$ ($\alpha = a, b, c$) values are also in good agreement with those found in literature; they are within a 7% deviation from the values determined previously by Ballet *et al.* (1989).

The second and more important quantity which can be determined from the high-temperature data (paramagnetic phase) is the ionic effective magnetic moment. This quantity is calculated from the slope of the linear portion of the experimental $\chi^{-1}(T)$ curve. Namely, in the temperature range where the Curie–Weiss law is obeyed, the effective magnetic moment of an atom/ion can be calculated from the Curie constant C as

$$\mu_{eff} = \sqrt{\frac{3k_B C}{N_A}} \simeq 2.827\sqrt{C}, \tag{2}$$

where k_B is the Boltzmann constant and N_A is Avogadro's number.

The experimental μ_{eff}^α ($\alpha = a, b, c$) values for the Co^{2+} ions in Co_2SiO_4 are presented in Table 1. The average moment μ_{eff}^{av} of $4.80 \pm 0.01 \mu_B$ is obtained from the fitting of the average magnetic susceptibility χ_{av}. The value of μ_{eff}^{av} found here is close to those of $4.77\mu_B$ and $4.87 \pm 0.10\mu_B$ reported by Hagemann *et al.* (2000) and Kondo & Miyahara (1966).

3.2.2. Magnetically ordered state. Around 50 K an anomaly in $\chi(T)$ is observed (Fig. 3) and below this temperature pronounced deviations from linearity in the $\chi^{-1}(T)$ plots occur. The appearance of a relatively sharp peak in the susceptibility indicates the onset of a long-range antiferromagnetic order and correlates well with the negative sign of the obtained Curie–Weiss temperatures θ_{CW} (Table 1).

The ordering temperature or Néel temperature T_N, determined by the temperature at the maximum (Kittel, 2005) of the $\chi(T)$ curves, is ~ 51 K. It should be noted that χ_b starts to drop rapidly at a slightly lower temperature of 49 K compared with that of 50 K for both χ_a and χ_c. The small difference of T_N for the three directions is consistent with the observation that the peak positions (which is another way to define T_N) in the curves of the derivative of the susceptibility, $d\chi/dT$, are located at 47 K for χ_b and 48 K in the case of χ_a and χ_c. In the specific heat measurements carried out on Co_2SiO_4 (Robie *et al.*, 1982), a sharp anomaly was also observed at ~ 50 K, which confirms the appearance of magnetic ordering.

The $\chi(T)$ curves in Fig. 3 show strong magnetic anisotropy not only above T_N (paramagnetic phase), but also below T_N (antiferromagnetically ordered phase). Below the transition temperature, χ_b decreases rapidly with decreasing temperature, but it does not approach zero. This behaviour is in contrast to the χ_a and χ_c curves which decrease only slightly when passing T_N and stay almost constant below 30 K. This result indicates that the easy axis for the antiferromagnetic ordering in Co_2SiO_4 is the b axis. This is in agreement with the results of Kato *et al.* (1995), where it was shown that magnetization along the b axis exhibits a metamagnetic-like double step transition at $H = 18$ T, while those of the a and c axes show no anomaly up to 19 T. Note that the anisotropy of

Table 2
The irreducible representations Γ_i and magnetic (Shubnikov) groups of *Pnma* associated with $\mathbf{k} = (0,0,0)$ as well as the corresponding magnetic modes along x, y, z for the 4a and 4c positions.

Representation	4a			4c			Magnetic group
	x	y	z	x	y	z	
Γ_1	G	C	A	.	C	.	*Pnma*
Γ_2	C	G	F	C	.	F	*Pn'm'a*
Γ_3	F	A	C	F	.	C	*Pnm'a'*
Γ_4	A	F	G	.	F	.	*Pn'ma'*
Γ_5	.	.	.	A	.	G	*Pn'm'a'*
Γ_6	.	.	.	.	A	.	*Pnma'*
Γ_7	.	.	.	.	G	.	*Pn'ma*
Γ_8	.	.	.	G	.	A	*Pnm'a*

Co_2SiO_4 is so strong that the magnetization along the *b* axis does not saturate at 4.2 K even with an external field of 41 T (Kato *et al.*, 1995).

The distinct difference in the temperature dependencies between the magnetic susceptibilities measured below T_N along different crystallographic directions is typical for antiferromagnetic single crystals. If an anisotropy precludes a rotation of the moments, a field applied along them gives rise to a susceptibility decreasing to zero when temperature decreases from T_N to 0 K ($\chi_{\parallel}$). When the field is perpendicular to the moments, the susceptibility remains nearly constant ($\chi_{\perp}$).

In Co_2SiO_4 the following general trend of $\chi(T)$ is observed. The susceptibility χ_b has a strong $\chi_{\parallel}$ character, whereas χ_a and χ_c are dominated by $\chi_{\perp}$. This indicates that the main direction of the magnetic moments is along the *b* axis. The non-zero value of χ_b at zero temperature is most probably caused by the canting of the magnetic moments. That is, the magnetic structure is expected to be non-collinear and the canting is responsible for a certain amount of $\chi_{\perp}$ in χ_b. Moreover, the slight decrease of both χ_a and χ_c below T_N is due to the presence of some $\chi_{\parallel}$ contribution in the susceptibilities along the *a* and *c* axes. The susceptibility $\chi_a(T)$ is lower than $\chi_c(T)$ indicating the smaller component of the total magnetic moment to be along the *a* axis.

3.2.3. Symmetry analysis of the magnetic structure. The thermal evolution of the experimental neutron powder diffraction patterns collected below 100 K with small temperature increments of 1 K is presented in Fig. 4. The neutron patterns show the appearance of new Bragg peaks at ~ 50 K, which are forbidden in the crystallographic space group *Pnma*. Allowed reflections are ($h00$) where $h = 2n$; ($0k0$): $k = 2n$; ($00l$): $l = 2n$; ($hk0$): $h = 2n$ and ($0kl$): $k + l = 2n$ (Hahn, 1995). Fig. 5 shows a typical neutron powder diffraction pattern of Co_2SiO_4 measured at 5 K as well as the results of the Rietveld refinement. The nuclear and magnetic structures were refined simultaneously in the antiferromagnetic region.

Along with anomalies observed in the specific heat (Robie *et al.*, 1982) and d.c. susceptibility measurements (Fig. 3), the presence of the new reflections can be attributed to the long-range magnetic ordering. The strongest pure magnetic reflections are (001), (100), (110) and (300); they are labelled

by M in Fig. 5. There is also an additional contribution to the intensity of the nuclear reflections, as can be seen, for instance, in the contribution to Bragg peaks at $2\theta \simeq 48.5°$ corresponding to (221) and (401). For the reflection (302) at $2\theta \simeq 57°$ about half of the intensity at 5 K is due to magnetic scattering.

All observed superstructure reflections can be indexed with a magnetic propagation vector $\mathbf{k} = (0, 0, 0)$. This means no loss in translational symmetry coming from the spin arrangement and identity of the magnetic and chemical cells. The chemical space group of Co_2SiO_4 remains *Pnma* down to 2.5 K according to our synchrotron and neutron diffraction data (Sazonov *et al.*, 2008). In this case, the propagation vector group G_k has the whole symmetry of the point group *mmm* (D_{2h}), which contains the rotational parts of the crystallographic space group *Pnma* (D_{2h}^{16}).

The eight magnetic Co ions per unit cell in Co_2SiO_4, which are distributed on two special 4a and 4c sites of the space group *Pnma*, produce two magnetic sublattices associated with these sites. In order to generate all possible magnetic structures that are compatible with the crystal structure, we have used the program for calculating irreducible representations *BASIREPS* from the *FULLPROF* suite (Rodríguez-Carvajal, 1993). In the framework of the representation analysis, which has been developed by Bertaut (1968), it was shown that there are only eight possible one-dimensional irreducible representations, Γ_i ($i = 1, 2, \ldots, 8$), of *mmm* associated with the propagation vector $\mathbf{k} = (0, 0, 0)$. They are summarized in Table 2 for the case of the crystallographic space group *Pnma*. The magnetic (Shubnikov) groups are also given together with the corresponding magnetic configurations for the 4a and 4c sites of *Pnma* (Table 2).
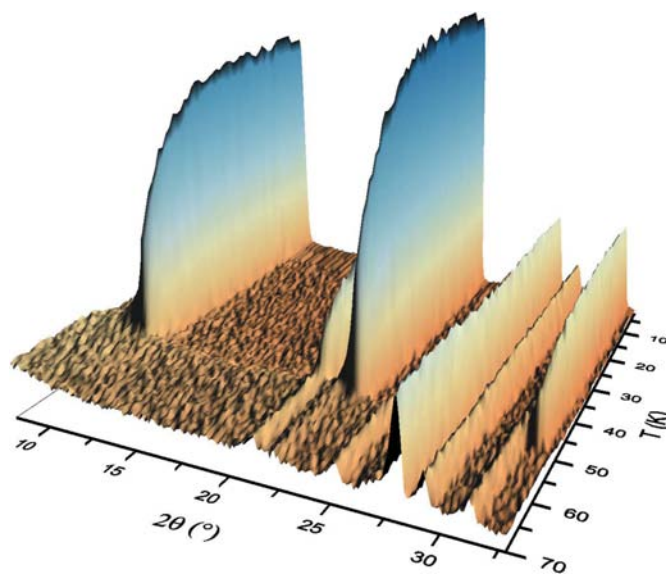

Figure 4
Thermal evolution of the neutron powder diffraction patterns of Co_2SiO_4 collected in the temperature range from 5 to 100 K with temperature increments of 1 K.

The fourfold positions (4a and 4c in our case) allow one ferromagnetic and three antiferromagnetic configurations or modes

$$F = S_1 + S_2 + S_3 + S_4,$$
$$G = S_1 - S_2 + S_3 - S_4,$$
$$A = S_1 - S_2 - S_3 + S_4,$$
$$C = S_1 + S_2 - S_3 - S_4, \qquad (3)$$

where S_n indicates the spin for the n-fold position.

This means that a vector F_x, for instance, has a maximum value when all the moments are aligned ferromagnetically and is zero for any antiferromagnetic combination. It characterizes a ferromagnetic $F(++++)$ configuration. In a similar manner, the G_x, A_x and C_x basis vectors as well as their y and z components can be obtained from (3). Finally, the sign change of the three magnetic moment projections μ_x, μ_y, μ_z for the sites 4a and 4c under those eight representations are listed in Table 3 (Schobinger-Papamantellos, 1978). The symbols $F(++++)$, $G(+-+-)$, $A(+--+)$ and $C(++--)$ correspond to Bertaut's notations (Bertaut, 1968).

Although there are no general extinction rules, the very strong intensities of the magnetic reflections (100) and (001) allow a preliminary statement to be made concerning the magnetic structure. First, we consider that both the Co1 and Co2 ions contribute to magnetism in Co_2SiO_4 and that the

basis functions for 4a and 4c belong to the same irreducible representation (this is usually the case). That is, we restrict the search to the magnetic structures having the highest possible symmetry. The representations from Γ_5 to Γ_8 exclude any magnetic moment on Co1 (Table 2) and cannot take part in the solution. The presence of the strong magnetic reflections (100) and (001) indicates that the primary component of the total magnetic moment is perpendicular to both the a and c axes at the same time. This is consistent with the b axis being the easy axis according to magnetic susceptibility measurements (see §3.2.2). Therefore, the contribution of Co2 to (100) and (001) can only appear due to the mode C_y taking into account the extinction rules for the 4c site (Gurewitz & Shaked, 1972, 1982; Gurewitz et al., 1974). The same conclusion can also be drawn for the 4a site according to the limiting conditions reported by Tezuka & Hinatsu (1998). Hence the only irreducible representation consistent with these considerations is Γ_1. This corresponds to the magnetic (Shubnikov) group Pnma which allows the antiferromagnetic configuration C_y for both 4a and 4c sites as well as additional antiferromagnetic G_x and A_z components in the case of 4a. This is also in agreement with the susceptibility measurements, which suggest the canted antiferromagnetic structure.

Good agreement between the observed and calculated intensities of the Co_2SiO_4 neutron diffraction patterns (see Fig. 5 as an illustration) indicates the correctness of the model used. Note that the single-crystal investigations make it possible to obtain higher accuracy in the determination of both the nuclear and magnetic structure parameters. Therefore, the neutron diffraction experiments on a single crystal were performed in order to verify the model of the Co_2SiO_4 magnetic structure at low temperature. A data collection at 2.5 K was performed up to $\sin\theta/\lambda \simeq 1.1$ Å^{-1} [λ = 0.552 (1) Å] and a total of 3226 Bragg reflection intensities was measured. After averaging 1424 independent reflections remained (R_{int} = 0.033). After applying the criterion $I > 2\sigma(I)$, 1070 observed reflections were used for the structure refinement. Our single-crystal neutron diffraction results are found to be in near-perfect agreement with the powder data.

If the spin components of the two different ions belong to two one-dimensional irreducible representations, different magnetic groups would be
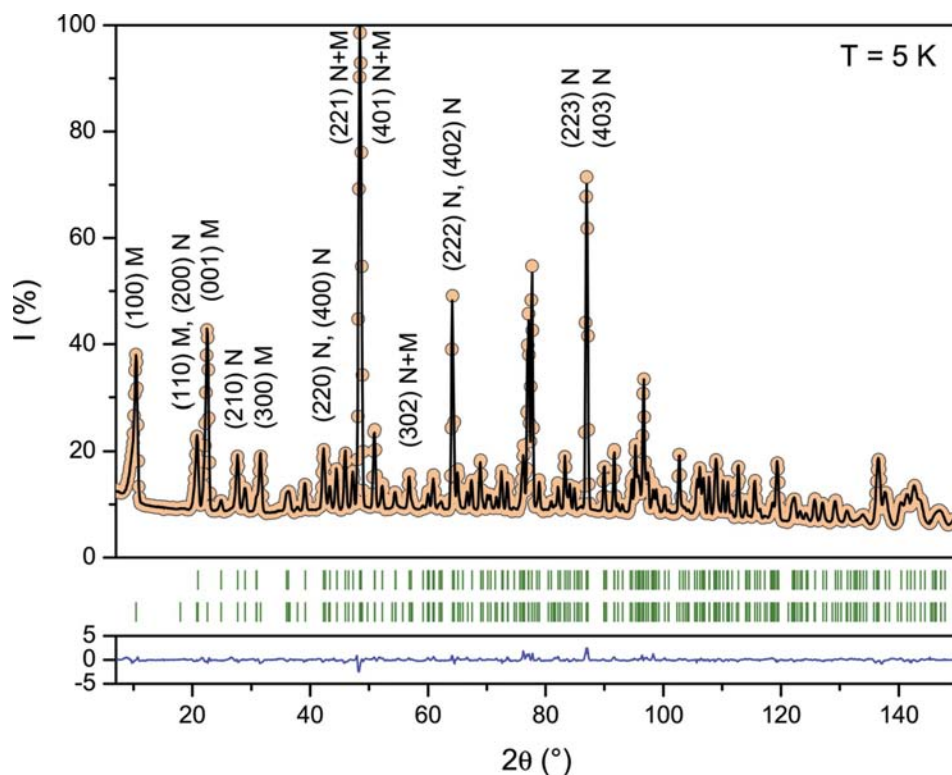

Figure 5
Neutron powder diffraction pattern (circles), Rietveld fit (upper continuous line) and allowed Bragg reflections (tick marks) for Co_2SiO_4 at 5 K. The lower trace is the difference, $I_{obs} - I_{calc}$, on the same scale. The upper row of the Bragg reflections shows the nuclear phase and the lower row represents the magnetic peaks. Some of the Bragg peaks are indexed. N and M denote the nuclear and magnetic contributions, respectively.

Table 3
The magnetic modes of the non-equivalent positions 4a and 4c for the eight possible magnetic space groups of *Pnma* associated with $\mathbf{k} = (0,0,0)$.

i	Position	*Pnma*			*Pn'm'a*			*Pnm'a'*			*Pn'ma'*		
	4a	G	C	A	C	G	F	F	A	C	A	F	G
1	$0, 0, 0$	+	+	+	+	+	+	+	+	+	+	+	+
2	$0, \frac{1}{2}, 0$	−	+	−	+	−	+	+	−	+	−	+	−
3	$\frac{1}{2}, \frac{1}{2}, \frac{1}{2}$	+	−	−	−	+	+	+	−	−	−	+	+
4	$\frac{1}{2}, 0, \frac{1}{2}$	−	−	+	−	−	+	+	+	−	+	+	−
	4c	.	C	.	C	.	F	F	.	C	.	F	.
1	$x, \frac{1}{4}, z$	.	+	.	+	.	+	+	.	+	.	+	.
2	$-x, \frac{3}{4}, -z$	.	+	.	+	.	+	+	.	+	.	+	.
3	$\frac{1}{2}+x, \frac{1}{4}, \frac{1}{2}-z$	.	−	.	−	.	+	+	.	−	.	+	.
4	$\frac{1}{2}-x, \frac{3}{4}, \frac{1}{2}+z$	.	−	.	−	.	+	+	.	−	.	+	.

i	Position	*Pn'm'a'*			*Pnma'*			*Pn'ma*			*Pnm'a*		
	4a	.	.	.	.	.	.	.	.	.	.	.	.
1	$0, 0, 0$	.	.	.	.	.	.	.	.	.	.	.	.
2	$0, \frac{1}{2}, 0$	.	.	.	.	.	.	.	.	.	.	.	.
3	$\frac{1}{2}, \frac{1}{2}, \frac{1}{2}$	.	.	.	.	.	.	.	.	.	.	.	.
4	$\frac{1}{2}, 0, \frac{1}{2}$	.	.	.	.	.	.	.	.	.	.	.	.
	4c	A	.	G	.	A	.	.	G	.	G	.	A
1	$x, \frac{1}{4}, z$	+	.	+	.	+	.	.	+	.	+	.	+
2	$-x, \frac{3}{4}, -z$	−	.	−	.	−	.	.	−	.	−	.	−
3	$\frac{1}{2}+x, \frac{1}{4}, \frac{1}{2}-z$	−	.	+	.	−	.	.	+	.	+	.	−
4	$\frac{1}{2}-x, \frac{3}{4}, \frac{1}{2}+z$	+	.	−	.	+	.	.	−	.	−	.	+

involved and the 'global magnetic symmetry' would be the intersection of these two magnetic groups. In that case a 'global Shubnikov group' is of lower symmetry than the Shubnikov groups associated with the representations of the individual ions. From the point of view of representation theory there is no conceptual difficulty in admitting that in the same crystallographic space group there might be spin components belonging to different representations. An example is TbFeO₃ (Bertaut *et al.*, 1967), where it was found at 1.5 K that the Fe spins are in the G_x mode belonging to Γ_4 or $Pb'n'm$ and the Tb spins are in a non-collinear A_xG_y arrangement belonging to Γ_8 or $Pbnm'$. These two magnetic groups have the intersection $P2_1'2_1'2_1$. Moreover, there are also examples where the interactions between ions of the same nature sited in non-equivalent crystallographic positions lead to a lower symmetry than that associated with their individual representations. For instance, in $Tb_5Si_{2.2}Ge_{1.8}$ the Tb atoms are distributed among two 8d and one 4c sites of the space group *Pnma*. Below 75 K the magnetic structure of this compound can only be described using the basis vectors of two different irreducible representations, Γ_3 and Γ_7 (Jiang & Guo, 2005).

Therefore, one can consider all the possible 32 intersections of four irreducible representations for the 4a site and eight representations for the 4c site. We have tested these variations and have found only a good agreement between fit and data for the intersections $G_xC_yA_z$ for Co1 as well as C_y for Co2. This again corresponds to Γ_1 or *Pnma* for both Co1 and Co2 and is in agreement with the single Néel temperature observed for Co₂SiO₄ in different experiments. The reliability factors for

this solution are at least ten times smaller than those for other configurations.

The magnetic structure of Co₂SiO₄ corresponding to the magnetic (Shubnikov) group *Pnma* is shown in Fig. 6. The magnetic moments of Co2 have a collinear arrangement along **b**, whereas the Co1 moments are canted with respect to all crystallographic axes. This confirms the magnetic model which was obtained by fitting the neutron diffraction data of Co₂SiO₄ collected at 4.2 K (Lottermoser & Fuess, 1988; Lottermoser *et al.*, 1986). However, in those works the magnetic moments on both Co sites were found to be similar ($3.90 \pm 0.10 \mu_B$ and $3.84 \pm 0.08 \mu_B$ for Co1 and Co2) in contrast to our results ($3.8 \pm 0.03 \mu_B$ and $3.35 \pm 0.02 \mu_B$ for Co1 and Co2, see Table 4).

The Cartesian (μ_x, μ_y and μ_z) and spherical (μ, ϕ and θ) components of both the Co1 and Co2 magnetic moments are given in Table 4. The canting angles for Co1 calculated from the refined magnetic moment values at 2.5 K are ~ 72, 21 and 80° with respect to the *a*, *b* and *c* axes.

3.2.4. Thermal evolution of the magnetic structure. First we consider the thermal evolution of the crystal structure of Co₂SiO₄ in terms of the Co—O interatomic distances and Co—O—Co angles which are involved in the superexchange magnetic interactions.

Increasing temperature causes a smooth, almost linear expansion of the average Co—O distance. The slope coefficients for the individual interatomic distances differ slightly from each other as well as from the average distance, but the difference is not significant taking into account the experimental uncertainty. In general, variations of the Co—O
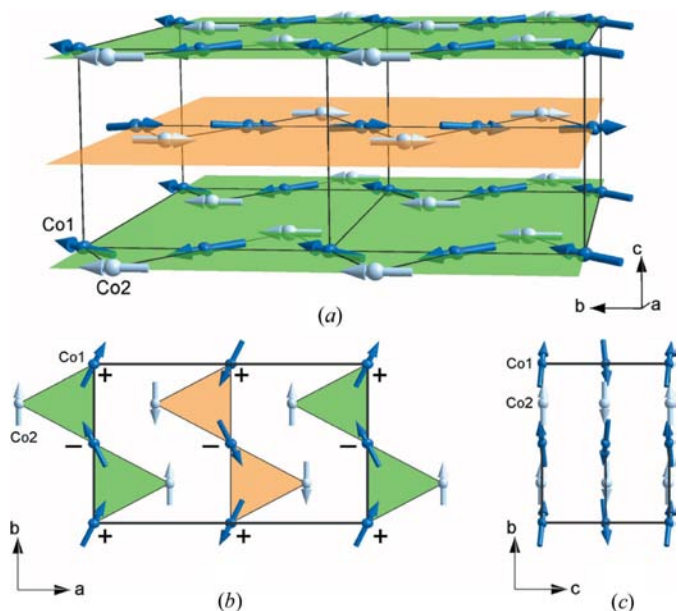

Figure 6
(*a*) Graphical representation of the magnetic structure of Co₂SiO₄ below 50 K. The non-magnetic atoms (Si and O) were excluded for simplicity. The figure shows the zigzag chains of Co in the layers perpendicular to the *c* axis. (*b*) Projection of the magnetic structure on the *ab* plane; the magnetic components out of the plane are identified by +/− signs. (*c*) Projection of the magnetic structure on the *bc* plane.

Table 4
The Cartesian (μ_x, μ_y and μ_z) and spherical (μ, ϕ and θ) components of the Co1 and Co2 magnetic moments according to the single-crystal neutron diffraction data at 2.5 K.

The directions of the magnetic moments for other cobalt ions in the unit cell could easily be obtained using the magnetic modes for the Schubnikov group *Pnma* (see Table 3).

	Co1 (0,0,0)	Co2 ($x,\frac{1}{4},z$)
M_x (μ_B)	1.20 ± 0.03	–
M_y (μ_B)	3.64 ± 0.02	3.35 ± 0.02
M_z (μ_B)	0.57 ± 0.09	–
M (μ_B)	3.87 ± 0.03	3.35 ± 0.02
ϕ (°)	71.8 ± 0.4	90
θ (°)	81.5 ± 1.2	90

$\chi^2 = 2.23$, $R[F^2 > 2\sigma(F^2)] = 0.033$, $wR(F^2) = 0.044$.

interatomic distances with temperature are smaller than 1%. The same is true for the O—Co—O angles (Fig. 7): most of them remain constant within experimental error. The powder neutron diffraction data are consistent with the single-crystal measurement. There might be a small indication of the magnetic phase transition near 50 K in the Co—O distances. However, the precision of atomic coordinates and hence interatomic distances is always reduced with respect to the determination of lattice parameters (Sazonov *et al.*, 2009).

Now we would like to consider the magnetic moments per Co^{2+} ion for the two cobalt sublattices, obtained from the neutron diffraction data. The temperature dependence of the magnetic moments per Co1 and Co2 ions is presented in Fig. 8. Besides the above-mentioned powder (P) and single-crystal (S1) measurements, additional single-crystal neutron diffraction experiments (S2) at several temperatures between 2 and 45 K were carried out. Here, only a limited number of Bragg
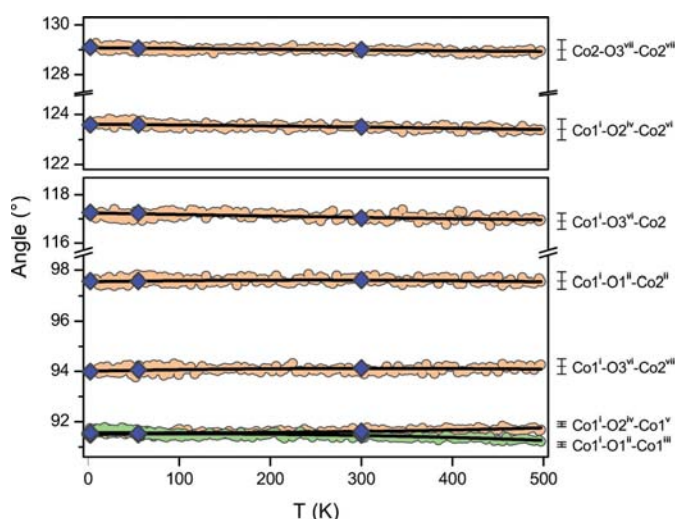
reflections with magnetic contribution was measured (from 23 to 95 reflections).

For a simple antiferromagnetic structure, the temperature dependence of the magnetic moment μ in the conventional molecular-field model can be expressed as

$$\frac{\mu}{\mu_0} = B_S\left(\frac{3S}{S+1} \frac{T_N}{T} \frac{\mu}{\mu_0}\right), \qquad (4)$$

where S is the spin of the system, μ_0 is the magnetic moment at $T = 0$ Å, and B_S is the Brillouin function

$$B_J(x) = \frac{2J+1}{2J} \coth\left(\frac{2J+1}{2J} x\right) - \frac{1}{2J} \coth\left(\frac{1}{2J} x\right). \quad (5)$$

In a first approach, we have attempted to fit the experimental data using the conventional molecular-field model with $S = 3/2$ [high-spin (HS) state of Co^{2+}, $t_{2g}^5 e_g^2$]. An important feature of the dependencies in Fig. 8 is a very sharp increase of μ just below the Néel temperature. The experimental magnetic moment values go much higher than the curve described by (4).

To compensate for this discrepancy, a modified molecular-field model (Beznosov *et al.*, 2002) was applied, which differs from the conventional form by the additional fitting parameters h and a

$$\frac{\mu}{\mu_0} = B_S\left(\frac{h}{T} + \frac{3S}{S+1} \frac{T_N[1 + a(\mu/\mu_0)]}{T} \frac{\mu}{\mu_0}\right), \qquad (6)$$

where h is a fictive magnetic-field modeling the effect of short-range magnetic order above T_N and a is a magnetoelastic parameter describing the magnetostrictive shift of T_N (Beznosov *et al.*, 2002; Fertman *et al.*, 2001).

Note that the magnetic anisotropy found in Co$_2$SiO$_4$ according to the magnetic susceptibility measurements (§3.2)
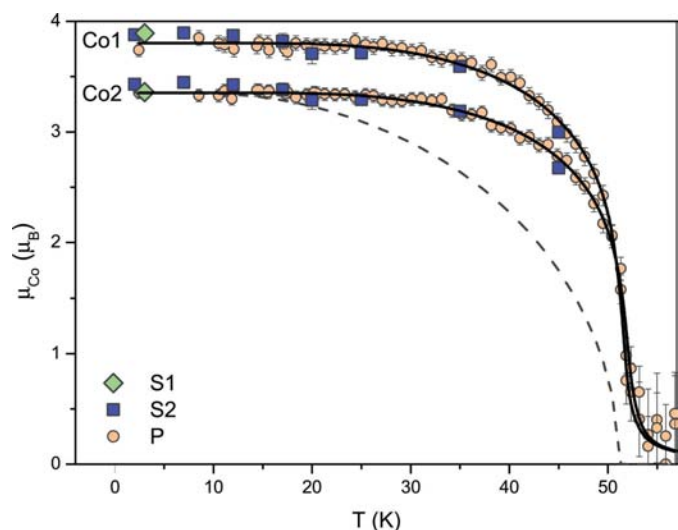

Figure 7
Temperature dependence of the Co—O—Co angles for Co$_2$SiO$_4$. Circles mark the results of the powder neutron diffraction measurements (error bars shown at the right), whereas rhombs mark the results of the single-crystal neutron diffraction measurements (error bars from the refinement are smaller than the symbols). The fits are used as guides to the eye. See Table 6 for the symmetry codes.

Figure 8
Temperature dependence of the Co magnetic moment for Co$_2$SiO$_4$. The experimental data from the single-crystal (S1,S2) and powder (P) neutron diffraction measurements are shown together with the fitting curves (solid lines) in a modified molecular-field model [equation (6)]. Error bars are smaller than the symbols if not given. The dashed line is shown to illustrate the deviation of $\mu_{Co2}(T)$ from the conventional molecular-field model [equation (4)].

Table 5
Coefficients from the fit of the experimental Co magnetic moment of Co_2SiO_4 in the modified molecular-field model [equation (6)] with $S = 3/2$.

	Co1 (0,0,0)	Co2 $(x, \frac{1}{4}, z)$
h	0.61 ± 0.18	0.63 ± 0.20
a	0.54 ± 0.04	0.54 ± 0.04
T_N (K)	49.9 ± 0.5	50.3 ± 0.6
M (μ_B)	3.84 ± 0.03	3.39 ± 0.03
$R†$	0.996	0.993

† According to equation (7).

in the paramagnetic phase also cannot be explained by the conventional molecular-field theory of antiferromagnetism, because such a theory would predict that $\chi_\alpha(T)$ ($\alpha = a, b, c$) curves coincide above T_N (Kittel, 2005). Thus, we fitted the magnetic moment $\mu(T)$ curves (Fig. 8) to the modified molecular-field model (6) for HS Co^{2+}. Table 5 summarizes the fitted parameters. For a rough estimate of how well the model fits the data we use the value R according to

$$R = 1 - \frac{\sum(I_{fit} - I_{obs})^2}{\sum(I_{obs} - \langle I_{obs}\rangle)^2}, \qquad (7)$$

where I_{obs} are the measured values and I_{fit} are the calculated values from the fit.

The fitted values of the parameters h and a for the Co1 curve are close to those for Co2. Therefore, the ordering with decreasing temperature evolves with almost the same velocity for the two magnetic sublattices, although they end up with different resultant magnetic moments per ion. The non-zero values of the parameter h are in agreement with the magnetic pre-ordering in Co_2SiO_4 above the Néel temperature, observed by means of the magnetic excitations measurements with neutron scattering (Schmidt et al., 1995).

The analysis of the neutron diffraction data as a function of temperature also shows that there is no change in the magnetic moment directions in the whole temperature range of the magnetically ordered state. As seen from Fig. 9 the Co1 canting angles in spherical representation (ϕ and θ) are independent of temperature within experimental error. This is in agreement with the strong magnetic anisotropy found in Co_2SiO_4 at least for the temperature range from 5 to 330 K (see §3.2).

3.2.5. Magnetic interactions. In order to find a relationship between the magnetic properties and the crystal structure of Co_2SiO_4 as well as to explain the negative sign of the Curie–Weiss temperatures, it is necessary to take into account the relative orientation of the magnetic moments on neighbouring magnetic sites. Since in Co_2SiO_4, all the cobalt–cobalt distances (≥ 3 Å) are much larger than those between cobalt and oxygen (2.09–2.22 Å), the direct exchange interactions (Co—Co) play a minor role. In indirect magnetic interactions between two cations via one bridge oxygen ion, the origin of the interaction lies in the existence of excited states of the cation–anion–cation configuration. In the excited configurations, one or both of the electrons in a 2p oxygen orbital are

excited into the empty, or partially filled, cation orbitals. The magnetic coupling between neighbouring Co^{2+} moments in Co_2SiO_4 can be understood by invoking the indirect super-exchange model of Kramers (1934) and Anderson (1950) taking also into account the Goodenough–Kanamori rules (Kanamori, 1959; Goodenough, 1963). It was shown that whenever octahedral-site cations are located on opposite sides of a common anion and the lines connecting the interacting cations to the intervening anion make an angle of 180°, cations interact antiferromagnetically if they have a half-filled e_g orbital. Note that Co^{2+} in the HS state ($t_{2g}^5 e_g^2$) has two half-filled e_g orbitals, namely $d_{x^2-y^2}$ and d_{z^2}. However, the case in which each cation is again surrounded octahedrally by anions, but the lines connecting the interacting cations to the intervening anion make an angle of 90°, often leads to a weak ferromagnetic coupling. That is, the superexchange becomes stronger with more open angles and shorter bond lengths, favoring the overlap between oxygen and metal orbitals and, thus enhancing the magnetic interactions.

In Co_2SiO_4 each Co1 ion is surrounded by eight near-neighbour cobalt ions (2 × Co1 and 6 × Co2), whereas there are ten near-neighbour cobalt ions (6 × Co1 and 4 × Co2) for every Co2 (see Fig. 2). The total number of the Co—O—Co paths is equal to 12 for both the Co1 and Co2 cations. All these exchange paths are described by seven indirect magnetic interactions (see Fig. 10) via oxygen anions giving rise to antiferromagnetic or ferromagnetic coupling (Table 6).

As can be seen from Table 6 the signs of exchange interactions Co—O—Co are in good agreement with the prediction of the Goodenough–Kanamori rules (Kanamori, 1959; Goodenough, 1963). Two types of indirect predominantly ferromagnetic couplings occur between the Co1 cations via O1 and O2. According to the single-crystal neutron diffraction measurements at 2.5 K, the Co1—Co1 distance is
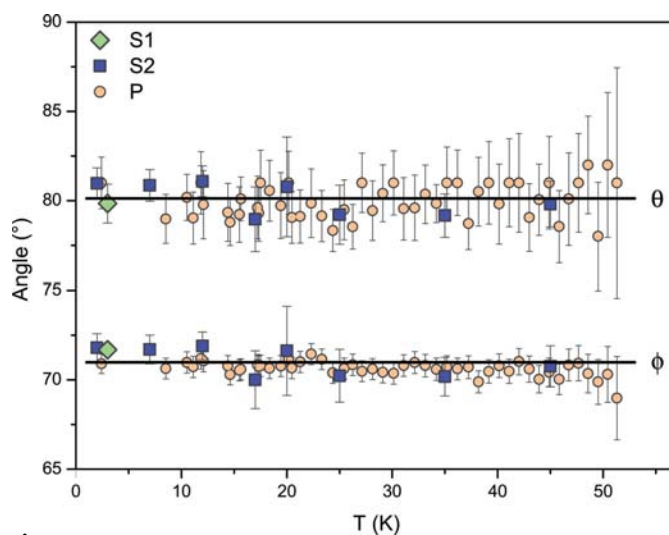

Figure 9
Temperature dependencies of the angles which describe the direction of the Co1 magnetic moment for Co_2SiO_4. The experimental data from the single-crystal (S1,S2) and powder (P) neutron diffraction measurements are shown. Error bars are smaller than the symbols if not given. The solid lines represent a linear fit.

Table 6
Interatomic distances (Å) and angles (°) in Co_2SiO_4 corresponding to the indirect exchange magnetic interactions (from single-crystal neutron diffraction measurements).

F denotes the ferromagnetic (positive) type of exchange interactions, whereas AF means antiferromagnetic (negative) coupling.

	Type	Co1†	Co2†	300 K	55 K	2.5 K
Between Co1 and Co1						
$Co1^i-O1^{ii}$, $Co1^{iii}-O1^{ii}$				2.0955 (2)	2.0907 (2)	2.0901 (2)
$Co1^i-O1^{ii}-Co1^{iii}$	F	2	–	91.48 (1)	91.48 (1)	91.47 (1)
$Co1^i-O2^{iv}$, $Co1^v-O2^{iv}$				2.0929 (2)	2.0896 (2)	2.0885 (2)
$Co1^i-O2^{iv}-Co1^v$	F	2	–	91.62 (1)	91.54 (1)	91.57 (1)
Between Co1 and Co2						
$Co1^i-O1^{ii}$				2.0955 (2)	2.0907 (2)	2.0901 (2)
$Co2^{ii}-O1^{ii}$				2.1813 (8)	2.1759 (6)	2.1756 (7)
$Co1^i-O1^{ii}-Co2^{ii}$	F	2	2	97.63 (3)	97.59 (2)	97.58 (3)
$Co1^i-O3^{vii}$				2.1715 (2)	2.1678 (1)	2.1691 (2)
$Co2^{viii}-O3^{vii}$				2.2250 (6)	2.2193 (5)	2.2194 (5)
$Co1^i-O3^{vii}-Co2^{viii}$	F	2	2	94.13 (1)	94.07 (2)	93.99 (3)
$Co1^i-O2^{iv}$				2.0929 (2)	2.0896 (2)	2.0885 (2)
$Co2^{vi}-O2^{iv}$				2.0731 (8)	2.0731 (6)	2.0751 (6)
$Co1^i-O2^{iv}-Co2^{vi}$	AF	2	2	123.50 (4)	123.59 (3)	123.59 (3)
$Co1^i-O3^{vii}$				2.1715 (2)	2.1678 (1)	2.1691 (2)
$Co2-O3^{vii}$				2.0684 (4)	2.0647 (4)	2.0629 (4)
$Co1^i-O3^{vii}-Co2$	AF	2	2	117.03 (3)	117.24 (2)	117.25 (3)
Between Co2 and Co2						
$Co2-O3^{vii}$				2.0684 (4)	2.0647 (4)	2.0629 (4)
$Co2^{viii}-O3^{vii}$				2.2250 (6)	2.2193 (5)	2.2194 (5)
$Co2-O3^{vii}-Co2^{viii}$	AF	–	4	129.00 (4)	129.05 (3)	129.09 (3)

Symmetry codes: (i) $x+\frac{1}{2}, -y+\frac{1}{2}, -z+\frac{1}{2}$; (ii) $x+\frac{1}{2}, -y+\frac{1}{2}, -z+\frac{3}{2}$; (iii) $-x+\frac{1}{2}, -y, z+\frac{1}{2}$; (iv) $-x+1, y+\frac{1}{2}, -z+1$; (v) $-x+\frac{1}{2}, -y+1, z+\frac{1}{2}$; (vi) $-x+1, y+\frac{1}{2}, -z+2$; (vii) $-x+\frac{1}{2}, y+\frac{1}{2}, z+\frac{1}{2}$; (viii) $-x+\frac{1}{2}, -y+1, z-\frac{1}{2}$. † Number of the near-neighbour exchange paths for Co1/Co2.

2.9936 (1) Å. The Co1—O1—Co1 and Co1—O2—Co1 angles have values of 91.47 (1) and 91.57 (1)°. Two types of interactions between Co1 and Co2 *via* O1 and O3 are also predominantly ferromagnetic. The Co1—Co1 distance is 3.2103 (6) Å. The Co1—O1—Co2 and Co1—O3—Co2 angles are 97.58 (3) and 93.99 (3)°. In addition, there are two types of predominantly antiferromagnetic coupling between Co1 and Co2 *via* O2 and O3. The Co1—Co2 distances are 3.6679 (7) and 3.6139 (7) Å, whereas Co1—O2—Co2 and Co1—O3—Co2 are 123.59 (3) and 117.25 (3)°. Finally, only one type of superexchange interaction is considered between the Co2 ions *via* O3, giving rise to a strong antiferromagnetic coupling. In this case, the Co2—Co2 distance is 3.8675 (7) Å and the Co2—O3—Co2 angle is 129.09 (3)°.

Thus, beside the four negative and four weak positive superexchange interactions between the Co1 and Co2 ions, there are four predominantly ferromagnetic Co1—O—Co1 paths weakening the overall antiferromagnetic behaviour. In contrast to Co1, the Co2 ions have four additional strong antiferromagnetic interactions. Therefore, the geometrical arrangement and the competition between the ferromagnetic and antiferromagnetic interactions seem to be responsible for

the canted magnetic structure of the Co1 sublattice in contrast to the collinear structure for Co2.

3.2.6. Magnetization density. In order to obtain further information on the magnetic properties of Co_2SiO_4, polarized neutron experiments were carried out. The classical polarized neutron flipping-ratio measurements (Nathans *et al.*, 1959) were used to study the magnetization distribution around magnetic atoms in ferromagnetic and paramagnetic materials. It is much more difficult to make such measurements in antiferromagnetic systems where the cross-section is not often polarization dependent and, therefore, the classical method is not applicable (Brown *et al.*, 1999). One way to study the magnetization density distribution in antiferromagnetic compounds is to perform polarized neutron flipping-ratio measurements in special conditions, namely above T_N in the paramagnetic state and in an applied external magnetic field. This gives information about the magnetization induced by the field and can help to understand the dominant magnetic interaction paths.

The flipping ratios R measured by polarized neutron diffraction are, for each Bragg reflection, the ratio between the intensity diffracted with spin up (I^+) and the intensity diffracted with spin down (I^-)

$$R = \frac{I^+}{I^-} = \frac{(F_N + \mathbf{F}_M^\perp)^2}{(F_N - \mathbf{F}_M^\perp)^2}, \qquad (8)$$

where F_N is the nuclear structure factor and $\mathbf{F}_M^\perp$ is the projection of the magnetic structure factor $\mathbf{F}_M$ into the scattering plane.

The sensitivity of the flipping-ratio method to the distribution of unpaired electrons in the unit cell is much greater than for the conventional method using a non-polarized beam. This is because of the additional term, which is only present when the beam is polarized. It couples nuclear and magnetic
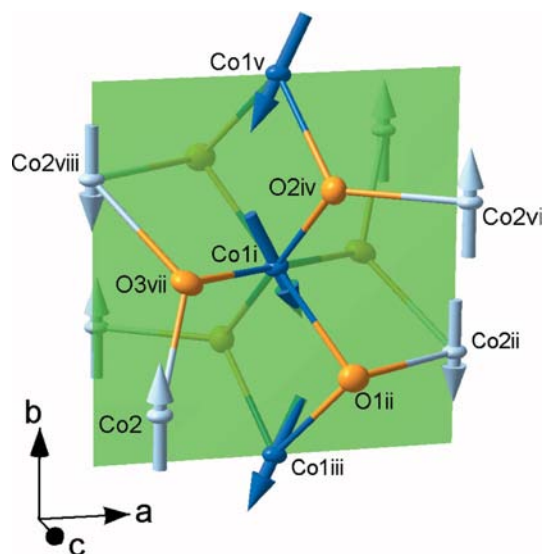

Figure 10
Graphical representation of a part of the Co_2SiO_4 magnetic structure showing the different exchange paths between the Co ions *via* O. See Table 6 for the symmetry codes.

scattering and is known as the nuclear-magnetic interference term.

For the data collection at 70 K, a total of 207 Bragg reflection flipping ratios for Co_2SiO_4 were measured up to $\sin\theta/\lambda \simeq 0.62$ Å^{-1} ($\lambda = 0.845$ Å). These yielded 113 independent reflections. A data collection at 150 K was also performed up to $\sin\theta/\lambda \simeq 0.62$ Å^{-1} and a total of 218 Bragg reflection flipping ratios were measured yielding 114 independent reflections. The average intensity of each set of equivalent reflections was calculated for up and down polarizations. Subsequently, we calculated the magnetic structure factor, assuming that the nuclear structure factor is known from our accurate non-polarized single-crystal neutron diffraction measurements.

For a graphical representation of the magnetization density, a Fourier inversion was initially applied to the experimental magnetic structure factors. The results of the Fourier inversion were compared with a maximum entropy reconstruction, which is another tool to study the density distribution. Both techniques gave similar results. However, in comparison to the Fourier map, the MEM map is more smooth, without any negative range, and seems to be more reliable.

Fig. 11 shows a projection of the magnetization densities in the Co_2SiO_4 unit cell along the b axis according to MEM. This projection was chosen because the experimental data are available only for the reflections with $k = 0, \pm1, \pm2$. The most prominent features of the map are regions of positive density close to the Co positions. Owing to a large preponderance of the cobalt magnetic moments, small details are not clearly visible on the conventional maps. However, by choosing an appropriate scale we were able to observe small but distinct peaks around the oxygen positions (see Fig. 11). This supports the assumption of a partly covalent character of the Co—O bonding and confirms that the superexchange interactions play a major role in the magnetic properties of Co_2SiO_4. Similar behaviour has already been reported by Lottermoser & Fuess (1992) in the case of another olivine, Mn_2SiO_4, where the occurrence of a magnetic moment of the O atoms has been shown.

Now we discuss the relative strength of the exchange interactions using the polarized neutron diffraction data. Above the antiferromagnetic phase transition ($T_N \simeq 50$ K), the influence of temperature destroys the long-range magnetic order. By applying an external magnetic field we introduce an additional term to the competition between the exchange interactions and temperature. As seen from Fig. 11 the influence of the external magnetic field differs for Co1 and Co2. It seems to be much easier to induce a ferromagnetic component in Co1 than for Co2. Thus, at 150 K in a magnetic field of 7 T applied parallel to the b axis the induced magnetic moment on Co2 is smaller than that of Co1. This is even more prominent at 70 K (closer to T_N). Therefore, we suggest that the exchange interactions between the Co1 ions *via* O are weaker compared with those between Co2. That is, the most important exchange interactions are antiferromagnetic and act through the paths Co2—O—Co2. This is in agreement with the Goodenough–Kanamori rules (Kanamori, 1959; Goodenough, 1963) considering the values of the Co2—O3—Co2 angle (Table 6). This exchange is the strongest in absolute value and is probably responsible for the overall antiferromagnetic behaviour of Co_2SiO_4.

4. Conclusions

Non-polarized neutron diffraction measurements on both single-crystal and powder samples show that the ordered magnetic structure of orthorhombic Co_2SiO_4 should be described as an antiferromagnetic arrangement of the Co^{2+} magnetic moments below $T_N \simeq 50$ K with a magnetic propagation vector $\mathbf{k} = (0, 0, 0)$. Detailed symmetry analysis of the magnetic structure shows that it corresponds to the magnetic (Shubnikov) group $Pnma$ which allows the antiferromagnetic configuration (G_x, C_y, A_z) for the $4a$ site with inversion symmetry $\bar{1}$ (Co1 position) and $(0, C_y, 0)$ for the $4c$ site with mirror symmetry m (Co2 position). This is in agreement with the magnetic susceptibility measurement $\chi(T)$, which also suggests a canted antiferromagnetic structure. The magnetic anisotropy was studied by fitting the observed $\chi(T)$ curves above T_N to the Curie–Weiss law. Thus, the Curie–Weiss temperatures θ_{CW} and effective magnetic moments μ_{eff} were obtained.

The magnetic moments from the neutron diffraction data were found to be $3.87 \pm 0.03\mu_B$ for Co1 and $3.35 \pm 0.02\mu_B$ for Co2. The value for Co1 is in excellent agreement with the literature data, whereas the value for Co2 is different (Lottermoser & Fuess, 1988). Note that the results of our measurements on samples prepared by different methods (powder and single crystal) and by using different instruments
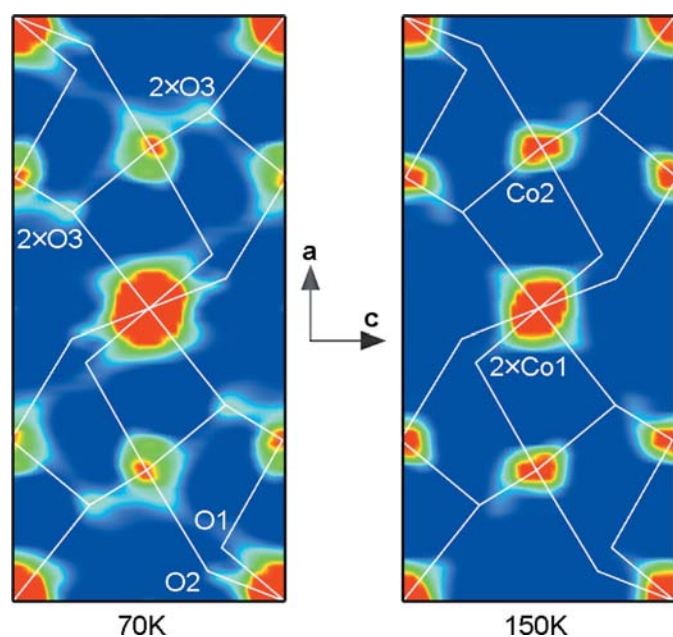

Figure 11
Maximum entropy reconstruction of the density corresponding to the observed magnetization distribution of Co_2SiO_4 with contour range from $0\mu_B$Å^3 (blue) to $2\mu_B$Å^3 (red). The projection of the unit cell along the b axis is shown.

(neutron powder and single-crystal diffractometers) are in good mutual agreement, indicating that the moments on Co1 and Co2 are different.

In order to follow the thermal evolution of the Co_2SiO_4 magnetic structure, the temperature dependence of the Co1 and Co2 magnetic moments obtained from neutron diffraction measurements was fitted in a modified molecular-field model. The results indicate the importance of introducing a magnetoelastic parameter describing the magnetostrictive shift of T_N and also show the magnetic pre-ordering above T_N. The precise analysis of the neutron diffraction data also shows that canting angles of the Co_2SiO_4 magnetic structure are independent of temperature, which is in agreement with the strong magnetic anisotropy found in Co-olivine.

Polarized neutron flipping-ratio measurements made at temperatures above T_N and with an external field of 7 T along the b axis were used to represent the magnetization density in the unit cell. The density maps revealed a non-negligible amount of magnetic moment on the oxygen positions indicating a delocalization of magnetic moment from Co towards neighbouring O owing to the superexchange interactions. The superexchange interactions $Co2-O-Co2$ are found to be much stronger than those between the Co1 ions and probably responsible for the overall antiferromagnetic behaviour of Co_2SiO_4.

References

Anderson, P. W. (1950). *Phys. Rev.* **79**, 350–356.

Ballet, O., Fuess, H., Wacker, K., Untersteller, E., Treutmann, W., Hellner, E. & Hosoya, S. (1989). *J. Phys. Condens. Matter*, **1**, 4955–4970.

Bertaut, E. F. (1968). *Acta Cryst.* A**24**, 217–231.

Bertaut, E. F., Chappert, J., Mareschal, J., Rebouillat, J. P. & Sivardière, J. (1967). *Solid State Commun.* **5**, 293–298.

Beznosov, A. B., Belevtsev, B. I., Fertman, E. L., Desnenko, V. A., Naugle, D. G., Rathnayaka, K. D. D. & Parasiris, A. (2002). *Low Temp. Phys.* **28**, 556–561.

Brown, P. J., Forsyth, J. B. & Tasset, F. (1999). *Physica B*, **267–268**, 215–220.

Cococcioni, M., Corso, A. D. & de Gironcoli, S. (2003). *Phys. Rev. B*, **67**, 094106–094106-7.

Fertman, E. L., Eremenko, V. V., Pal-Val, P. P., Popov, V. P. & Chebotayev, N. N. (2001). *Low Temp. Phys.* **27**, 320–324.

Goodenough, J. B. (1963). *Magnetism and the Chemical Bond.* New York: John Wiley and Sons, Inc.

Gurewitz, E., Makovsky, J. & Shaked, H. (1974). *Phys. Rev. B*, **9**, 1071–1076.

Gurewitz, E. & Shaked, H. (1972). *Acta Cryst.* A**28**, 280–284.

Gurewitz, E. & Shaked, H. (1982). *Acta Cryst.* B**38**, 2771–2775.

Hagemann, I. S., Khalifah, P. G., Ramirez, A. P. & Cava, R. J. (2000). *Phys. Rev. B*, **62**, R771–R774.

Hahn, T. (1995). Editor. *International Tables for Crystallography*, Vol. A. Dordrecht: Kluwer Academic Publishers.

Haiber, M., Ballone, P. & Parrinello, M. (1997). *Am. Mineral.* **82**, 913–922.

Henderson, C. M. B., Redfern, S. A. T., Smith, R. I., Knight, K. S. & Charnock, J. M. (2001). *Am. Mineral.* **86**, 1170–1187.

Jiang, X. F. & Guo, G. Y. (2004). *Phys. Rev. B*, **69**, 155108–155108-6.

Jiang, X. F. & Guo, G. Y. (2005). *Phys. Rev. B*, **72**, 104431–104431-9.

Kanamori, J. (1959). *J. Phys. Chem. Solids*, **10**, 87–89.

Kato, H., Untersteller, E., Hosoya, S., Kido, G. & Treutmann, W. (1995). *J. Magn. Magn. Mater.* **140–144**, 1535–1536.

Kittel, C. (2005). *Introduction to Solid State Physics*, 8th ed. New York: Wiley.

Kondo, H. & Miyahara, S. (1966). *J. Phys. Soc. Jpn*, **21**, 2193–2196.

Kramers, H. A. (1934). *Physica*, **1**, 182–192.

Lin, C. C. (2001). *J. Solid State Chem.* **157**, 102–109.

Lottermoser, W. & Fuess, H. (1988). *Phys. Status Solidi A*, **109**, 589–595.

Lottermoser, W. & Fuess, H. (1992). *Phys. Chem. Miner.* **19**, 46–51.

Lottermoser, W., Müller, R. & Fuess, H. (1986). *J. Magn. Magn. Mater.* **54–57**, 1005–1006.

Meven, M., Hutanu, V. & Heger, G. (2007). *Neutron News*, **18**, 19–21.

Nathans, R., Shull, C. G., Shirane, G. & Andresen, A. (1959). *J. Phys. Chem. Solids*, **10**, 138.

Nomura, S., Santoro, R., Fang, J. & Newnham, R. (1964). *J. Phys. Chem. Solids*, **25**, 901–905.

Rinaldi, R., Gatta, G. D., Artioli, G., Knight, K. S. & Geiger, C. A. (2005). *Phys. Chem. Miner.* **32**, 655–664.

Robie, R. A., Hemingway, B. S. & Takei, H. (1982). *Am. Mineral.* **67**, 470–482.

Rodríguez-Carvajal, J. (1993). *Physica B*, **192**, 55–69.

Sakata, M., Uno, T., Takata, M. & Howard, C. J. (1993). *J. Appl. Cryst.* **26**, 159–165.

Sazonov, A., Hutanu, V., Meven, M., Heger, G., Hansen, T. & Senyshyn, A. (2009). In preparation.

Sazonov, A., Meven, M., Hutanu, V., Kaiser, V., Heger, G., Trots, D. & Merz, M. (2008). *Acta Cryst.* B**64**, 661–668.

Schmidt, W., Brotzeller, C., Schweiss, P., Tietze-Jaensch, H., Geick, R. & Treutmann, W. (1995). *J. Magn. Magn. Mater.* **140–144**, 1989–1990.

Schobinger-Papamantellos, P. E. (1978). *J. Phys. Chem. Solids*, **39**, 197–205.

Tezuka, K. & Hinatsu, Y. (1998). *J. Solid State Chem.* **141**, 404–410.

Wilke, M., Farges, F., Petit, P. E., Brown, G. E. & Martin, F. (2001). *Am. Mineral.* **86**, 714–730.